ISSN 0915-633X

NATIONAL INSTITUTE FOR FUSION SCIENCE

Plasma Transport Simulation Modeling for Helical Confinement Systems

K. Yamazaki and T. Amano

(Received – July 15, 1991)

NIFS-104

Aug. 1991

RESEARCH REPORT
NIFS Series

This report was prepared as a preprint of work performed as a collaboration research of the National Institute for Fusion Science (NIFS) of Japan. This document is intended for information only and for future publication in a journal after some rearrangements of its contents.

Inquiries about copyright and reproduction should be addressed to the Research Information Center, National Institute for Fusion Science, Nagoya 464-01, Japan.

NAGOYA, JAPAN

Plasma Transport Simulation Modeling for Helical Confinement Systems

K.YAMAZAKI and T.AMANO

National Institute for Fusion Science,
Chikusa-ku, Nagoya 464-01,Japan

ABSTRACT

New empirical and theoretical transport models for helical confinement systems are developed based on the neoclassical transport theory including the effect of radial electric field and multi-helicity magnetic components, and the drift wave turbulence transport for electrostatic and electromagnetic modes, or the anomalous semi-empirical transport. These electron thermal diffusivities are compared with CHS (Compact Helical System) experimental data, which indicates that the central transport coefficient of the ECH plasma agrees with the neoclassical axi-symmetric value and the transport outside the half radius is anomalous. On the other hand, the transport of NBI-heated plasmas is anomalous in the whole plasma region. This anomaly is not explained by the electrostatic drift wave turbulence models in these flat-density-profile discharges.

For the detailed prediction of plasma parameters in LHD (Large Helical Device), 3-D(dimensional) equilibrium/1-D transport simulations including empirical or drift wave turbulence models are carried out, which suggests that the global confinement time of LHD is determined mainly by the electron anomalous transport near the plasma edge region rather than the helical ripple transport in the core region. Even if the ripple loss can be eliminated, the increase of the global confinement is 10 %. However, the rise in the central ion temperature is more than 20 %. If the anomalous loss can be reduced to the half level of the present scaling, like so-called "H-mode" of the tokamak discharges, the neoclassical ripple loss through the ion channel becomes important even in the plasma core. The 5 % radial inward shift of the plasma column with respect to the major radius is effective for improving plasma confinement and raising more than 50 % of the fusion product by reducing this neoclassical asymmetric ion transport loss and increasing 10 % in the plasma radius.

KEYWORDS: equilibrium-transport simulation, neoclassical transport, anomalous transport, drift wave turbulence, empirical transport scaling, LHD(Large Helical Device), CHS(Compact Helical System)

1. INTRODUCTION

Helical confinement configurations[1] have distinct advantages in realizing steady-state operations without current drive and plasma current disruptions. To demonstrate these advantages, the Large Helical Device (LHD) with a superconducting magnetic coil system[2, 3,4] is under construction. The present confinement properties in these helical systems might be within the so-called "L-mode" range of Tokamak transport, and the confinement improvement is one of urgent issues for helical confinement systems as well as for tokamak systems. Moreover, helical systems are supposed to suffer from serious helical ripple diffusions in the high temperature plasma regime, different from tokamak systems. So far, the empirical scaling law (so-called "LHD scaling") [5] of the global confinement time was obtained based on several stellarator/heliotron experiments, and the Gyro-reduced Bohm scalings was discussed[6] for the modification of the LHD scaling in the high density regime. The past and present medium-sized experiments[7,8] suggest that the transport outside the half minor radius is anomalous and the transport near the center is neoclassical for ECH plasma. In NBI-heated plasmas, however, the whole region is anomalous. The spatial dependence of the empirical thermal diffusivity is also attempted to obtain[9,10].

In next-generation large helical machines with high temperature plasmas, the neoclassical ripple transport might be important even in the core region. In this paper, a new simulation model for the equilibrium-transport in the helical confinement systems is developed including the effect of the change in the plasma equilibrium and the magnetic structure on the neoclassical transport. However, without knowing the radial dependences of anomalous transport coefficients, it is impossible to predict whether the effect of this ripple transport is predominant or not, compared with anomalous transport. A new model for empirical "local" thermal conductivities is proposed to forecast the future experiments in LHD (major radius $R \sim$4m, magnetic field $B \sim$4T, plasma minor radius $a_p \sim$ 0.6m).

In Section 2, the neoclassical model of transport coefficients is described. In Section 3, the anomalous transport models based on the drift wave turbulences and also empirical thermal diffusivities are presented in detail. In Section 4, the validity of these anomalous thermal diffusivities is checked using CHS experimental data. A one-dimensional transport simulation modeling coupled with 3-dimensional plasma equilibrium and its simulation results for LHD plasmas are given in Section 5. Lastly, Section 6 summarizes our conclusions.

2. NEOCLASSICAL MODELS OF THERMAL CONDUCTIVITIES

The neoclassical transport losses in helical plasma configurations are divided into axi-symmetric(SYM) tokamak-like part[11,13] and asymmetric(ASY) helical-ripple part [12,14]. Effects of the radial electric field E_ρ ($= -e\partial\Phi/\partial\rho$) are included in the ripple transport simulation[15]. Multiple-helicity effects of the magnetic field configuration[16] are taken into account in the $1/\nu$ regime by introducing the form factor ratio of multi-helicity case to the single helicity case, F_m/F_s. Multiple helicity form factor F_m is calculated by using "GIOTA" code[17]. Asymmetric particle and heat fluxes, Γ_{ASYa} and Q_{ASYa}, of species a (electron (a=e) or ion (a=i)) as a function of flux-averaged radial variable ρ are given[12] by

$$\Gamma_{ASYa} = -\epsilon_t^2 \epsilon_h^{1/2} v_{da}^2 n_a \int_0^\infty dx x^{5/2} e^{-x} \frac{\tilde{\nu}_a(x) A_a(x)}{\omega_a^2(x)}, \tag{1}$$

$$Q_{ASYa} + \frac{5}{2}\Gamma_{ASYa} T_a = -\epsilon_t^2 \epsilon_h^{1/2} v_{da}^2 n_a T_a^2 \int_0^\infty dx x^{7/2} e^{-x} \frac{\tilde{\nu}_a(x) A_a(x)}{\omega_a^2(x)}, \tag{2}$$

where

$$A_a(x) = \frac{1}{n_a}\frac{\partial n_a}{\partial \rho} - \frac{Z_a}{T_a} E_\rho + (x - \frac{3}{2})\frac{1}{T_a}\frac{\partial T_a}{\partial \rho} \tag{3}$$

$$\tilde{\nu}_a(x) = \nu_a^0 x^{-1.5} \epsilon_h^{-1} [[(1 - \frac{1}{2x}) erf(x^{1/2}) + \frac{1}{(\pi x)^{1/2}} e^{-x}] + \tilde{z}_a] \tag{4}$$

$$x = \frac{m_a v_{tha}^2}{2T_a} \tag{5}$$

$$\omega_a^2(x) = 2.21 \frac{\tilde{\nu}_a^2}{F_m/F_s} + 1.5(\epsilon_t/\epsilon_h)^{1/2}(\omega_E + \omega_{Ba})^2 + (\epsilon_t/\epsilon_h)^{3/2}[\frac{\omega_{Ba}}{4} + 0.6|\omega_{Ba}|\tilde{\nu}_a(x)(\epsilon_h/\epsilon_t)^{3/2}] \tag{6}$$

$$\nu_a^0 = \frac{4\pi e^4 n_a \ln\Lambda}{m_a^2 v_{tha}^3} \tag{7}$$

Here, ϵ_t, ϵ_h, n_a, T_a, v_{da}, v_{tha}, ω_E and ω_{Ba} are toroidal inverse aspect ratio (ρ/R), helical ripple modulation, plasma density, plasma temperature, toroidal drift velocity, thermal velocity, ExB drift and ∇B drift frequencies, respectively. The collission frequency $\tilde{\nu}_a$ is $\tilde{\nu}_e = \nu_{ee} + \nu_{ei}$ with $\tilde{z}_e = Z_{eff}$ for electrons and $\tilde{\nu}_i = \nu_{ii}$ with $\tilde{z}_i = 0$ for ions. In the above equations, the ν regime transport was modified according to Ref.[14]. The radial electric profile is determined by the balance between the asymmetric electron and ion loss fluxes,

$$\Gamma_{ASYe}(E_\rho) = \Gamma_{ASYi}(E_\rho). \tag{8}$$

The validity of these multi-helicity neoclassical transport has been examined by using the DKES code [18].

3. ANOMALOUS MODELS OF THERMAL CONDUCTIVITIES

3.1 Drift Wave Turbulence (DWT) Models

(1) Electrostatic DWT Models

The drift wave turbulence (DWT) models have been successfully applied to simulate tokamak discharges [19,20]. The electrostatic models related to δExB/B^2 turbulent diffusion with long wavelength ($k_\perp \rho_s \sim 1/3$; $k_\perp$ being the perpendicular wave length and ρ_s the ion Lamor radius with the ion sound velocity $(T_e/M_i)^{1/2}$) consist of electron or ion modes; collisionless or dissipative modes; and cylindrical, toroidal or helical modes. The diffusion coefficient of circulating electron (CE) mode for collisionless (CCE, $\nu_{ei} < \omega_{tet}$) or collisional (XCE, $\omega_{tet} < \nu_{ei}$) regime is given by

$$D_{CE} = \max(D_{CCE}, D_{XCE}) \tag{9}$$

$$D_{CCE} = \frac{\omega_{*e}}{k_\perp^2}\frac{\omega_{*e}}{\omega_{tet}} \tag{10}$$

$$D_{XCE} = \frac{\omega_{*e}}{k_\perp^2}\frac{\omega_{*e}}{\omega_{tet}}\frac{\nu_{ei}}{\omega_{tet}}. \tag{11}$$

where, $\omega_{*e} = k_\perp T_e/L_n eB$ ($L_n = n\ /n'$ is the characteristic density length) and $\omega_{tet} = v_{the}(\epsilon/R)$ are electron diamagentic frequency and electron toroidal transit frequency, respectively.

On the other hand, the toroidally trapped electron (TEt) mode diffusion of collisionless (CTEt, $\nu_{efft} < \omega_{*e}$) or dissipative (DTEt, $\omega_{*e} < \nu_{efft} < \omega_{tet}$) mode is

$$D_{TEt} = \min(D_{CTEt}, D_{DTEt}) \tag{12}$$

$$D_{CTEt} = \epsilon_t^{1/2}\frac{\omega_{*e}}{k_\perp^2} \tag{13}$$

$$D_{DTEt} = \epsilon_t^{1/2}\frac{\omega_{*e}}{k_\perp^2}\frac{\omega_{*e}}{\nu_{efft}}, \tag{14}$$

where $\nu_{efft} = \nu_{ei}/\epsilon_t$ is effective toroidal collision frequency. The "Gyro-Reduced Bohm (GRB)" scaling[21] coincides with this CTE mode by omitting ϵ_t-dependence:

$$D_{GRB} = \frac{\omega_{*e}}{k_\perp^2} = D_{CTEt}\epsilon_t^{-1}. \tag{15}$$

In addition to these cylindrical and toroidal electrostatic DWT model, we added helical ripple contributions (ϵ_h: helical ripple) of the collisionless (CTEh, $\nu_{effh} < \omega_{*e}$) and dissipative (DTEh, $\omega_{*e} < \nu_{effh} < \omega_{teh}$) mode:

$$D_{TEh} = \min(D_{CTEh}, D_{DTEh}) \tag{16}$$

$$D_{CTEh} = \epsilon_h^{1/2} \frac{\omega_{*e}}{k_\perp^2} \tag{17}$$

$$D_{DTEh} = \epsilon_h^{1/2} \frac{\omega_{*e}}{k_\perp^2} \frac{\omega_{*e}}{\nu_{effh}}. \tag{18}$$

where, the effective helical collision frequency ν_{effh} and the electron helical transit frequency ω_{teh} are given by

$$\nu_{effh} = \nu_{ei}/\epsilon_h,$$
$$\omega_{teh} = v_{the} \frac{M}{R},$$

respectively, with helical ripple ϵ_h, helical mode number M and electron thermal velocity $v_{the} = (2T_e/m_e)^{1/2}$.

As for ion mode, the ion temperature gradient (ITG) turbulence is important especially for flat density profiles:

$$D_{ITG} = \frac{\omega_{*e}}{k_\perp^2} (2\frac{T_i}{T_e}\eta_i \frac{L_n}{R})^{1/2} f_{ITGth} \tag{19}$$

$$f_{ITGth} = (1 + \exp(-6(\eta_i - \eta_{th})))^{-1} \tag{20}$$

$$\eta_i = \frac{L_n}{L_{Ti}} = \frac{n/n'}{T_i/T_i'} \tag{21}$$

We adopt the total anomalous transport coefficients due to electrostatic DWT modes as:

$$D_{ANe} = c_{CE} D_{CE} + c_{TEt} D_{TEt} + c_{TEh} D_{TEh} \tag{22}$$

$$\chi_{ANe} = \frac{5}{2} D_{ANe} (1 + 3c_{ei} \frac{L_n}{R} \eta_i f_{ITGth}) \tag{23}$$

$$\chi_{ANi} = \frac{5}{2} (c_{ie} D_{ANe} + c_{ITG} D_{ITG}) \tag{24}$$

The coefficients $c_{CE}, c_{TEt}, c_{TEh}, c_{ei}, c_{ie}$ and c_{ITG} are usually set to zero or unity in this paper.

(2) Electromagnetic DWT Models

Different from the long-wave-length turbulence, the electromagnetic drift wave has short wave length of collisionless skin depth c/ω_{pe} and gives rise to $v_\parallel \delta B/B$ diffusion. The diffusion coefficient is given for tokamak systems (EMt)[22] and is extended to the helical (EMh) modes as:

$$D_{ANe} = c_{EMt} D_{EMt} + c_{EMh} D_{EMh} \tag{25}$$

$$D_{EMt} = \epsilon_t^{1/2} (\frac{c}{\omega_{pe}})^2 \omega_{bet} \tag{26}$$

$$D_{EMh} = \epsilon_h^{1/2} (\frac{c}{\omega_{pe}})^2 \omega_{beh} \tag{27}$$

$$\chi_{ANe} = \frac{5}{2} D_{ANe} \tag{28}$$

$$\chi_{ANi} = \frac{5}{2} c_{ie} D_{ANe} \tag{29}$$

where electron bounce frequencies, ω_{bet} and ω_{beh}, are

$$\omega_{bet} = \epsilon_t^{1/2} v_{the} \frac{t}{R},$$

and

$$\omega_{beh} = \epsilon_h^{1/2} v_{the} \frac{M}{R}.$$

This electromagnetic mode in tokamaks is similar to the Ohkawa model[23]

$$D_{Ohkawa} = (\frac{c}{\omega_{pe}})^2 \omega_{tet} = D_{EMt} \epsilon_t^{-1} \tag{30}$$

which has successfully explained the Alcator scalings.

The schematic drawing of the DWT mode transport coefficients is given in FIG.1.

3.2 Empirical, Anomalous Transport Models

In helical systems the transport process is anomalous as in tokamaks, and the empirical scaling of global confinement time $\tau_{E,emp}$(s) for helical systems (so called "LHD scaling"[5]) is given by

$$\tau_{E,emp} = 0.17 f_{enh} P_{MW}^{-0.58} n_{20}^{0.69} B_T^{0.84} R_m^{0.75} a_m^2 \tag{31}$$

where, P_{MW}, n_{20}, B_T, R_m and a_m are total absorbed heating power (MW), average plasma density (10^{20} m $^{-3}$), magnetic field strength (T), major plasma radius (m) and minor plasma radius (m), respectively. We take into account the confinement improvement by an enhancement factor f_{enh}. As for local transport coefficient $\chi(\rho)$ (m^2/s) as a function of flux-averaged radial variable ρ, the Heliotron-E scaling[9] near the position of r/a_p=2/3 (a_p:plasma radius) was deduced as

$$\chi_{H-E}(\rho) = 30.6 B_T^{-2.0} T_{keV}(\rho)^{1.52}. \tag{32}$$

On the other hand, the W7-AS semi-local χ scaling[10] was derived by using total absorbed heating power P:

$$\chi_{W7-AS}(\rho) = 0.64 P_{MW}^{0.76} B_T^{-0.60} n_{20}(\rho)^{-0.95} \iota^{-0.49}. \tag{33}$$

The former $\chi(\rho)$ scaling is only valid in the half-radius region, and both scalings do not include the major radius dependence which is important to estimate future machine performances.

By using the relation $\chi(\rho) \sim \rho^2/4\tau_E(\rho)$, we define a new scaling for semi-local thermal diffusivity as a combination of $n(\rho)\&T(\rho)$-dependent diffusivity $\chi_1(\rho)$ and $n(\rho)$-dependent diffusivity $\chi_2(\rho)$ with P-dependent coefficient:

$$\chi_{emp}(\rho) = \chi_1^s \chi_2^{(1-s)} \tag{34}$$

$$\chi_1(\rho) = 15.8 f_{enh}^{-2.38} B_T^{-2.0} R_m^{-0.40} T(r)_{keV}^{1.38} n_{20}(\rho)^{-0.26} \tag{35}$$

and

$$\chi_2(\rho) = 1.47 f_{enh}^{-1} P_{MW}^{0.58} B_T^{-0.84} R_m^{-0.75} n_{20}(\rho)^{-0.69}. \tag{36}$$

where, s is an adjusting parameter to fit the experimental data. The radial profile of $\chi_1(\rho)$ decreases outward due to temperature dependence, and does not reproduce experimental profile data. On the other hand, the coefficient $\chi_2(\rho)$ depends only on the density profile and increases outward, but still disagrees with the experimental data. The proper s value is $0 \lesssim s \lesssim 0.5$ as shown in Section 4. The ECH plasma with the central neoclassical transport and the outer anomalous property corresponds to $s \sim 0.3 - 0.5$. The anomalous transport in the whole plasma region as NBI plasmas is described by $s \sim 0 - 0.2$. This semi-local coefficient can reproduce experimental profiles.

The another model (local model) is to add the spatial factor $g(\rho)$ on the local value χ_1

$$\chi_{emp}(\rho) = \chi_1 g(\rho) \tag{37}$$

for example,

$$g(\rho) \propto (1 + 10.0\rho^{8.0})^{1.0}$$

or

$$g(\rho) \propto (1.1 - \rho^{2.0})^{-1.0}.$$

These coefficients are chosen to fit the experimental data.

4. COMPARISONS WITH CHS EXPERIMENTAL DATA

The transport coefficients described in the previous section are compared with typical experimental data of two ECH plasma discharges and one NBI-heated discharge[8] in CHS (Compact Helical System, helical period M=8, major radius R= 1.0 m, magnetic field B= 1.5 T). The experimentally obtained density and temperature profiles of (a) low density and (b) medium density ECH discharges are approximated by the following forms:

(a) low n_e ECH case (0.9T magnetic field, 180kW absorbed heating power)

$$n_e[10^{12}cm^{-3}] = (4.0 - 0.5)(1 - \rho^2)^{1.5}(1 + 3.5\rho^2) + 0.5$$

$$T_e[eV] = (900 - 100)(1 - \rho^{1.5})^3 + 100$$

$$T_i[eV] = (100 - 20)(1 - \rho^2) + 20,$$

(b) medium n_e ECH case (0.95T magnetic field, 63kW absorbed heating power)

$$n_e[10^{12}cm^{-3}] = (8.0 - 1.0)(1 - \rho^2)^{1.5}(1 + 3.5\rho^2) + 1.0$$

$$T_e[eV] = (400 - 50)(1 - \rho^{1.5})^3 + 50$$

$$T_i[eV] = (80 - 10)(1 - \rho^2) + 10.$$

The profile of the NBI-heated discharge is given by:

(c) NBI case (1.5T, 1.1MW NBI)

$$n_e[10^{13}cm^{-3}] = (2.5 - 0.5)(1 - \rho^4)(1 + \rho^2) + 0.5$$

$$T_e[eV] = (450 - 20)(1 - \rho^{1.5}) + 20$$

$$T_i[eV] = (200 - 20)(1 - \rho^2) + 20.$$

All these density profiles are hollow type. The calculated transport coefficients are shown in FIG.2 and compared with experimental data. The neoclassical values of symmetric (SYM) and asymmetric transport (ASY) parts are also plotted in this figure. The radial electric field E_ρ plotted in this figure is obtained from Eq.(8). These calculated radial electric fields agree with experimental values in the plasma core except near the plasma surface[24] . The helical-ripple asymmetric transport near the edge might be smaller than this plot because of the higher electric field than expected. The ripple transport estimated here includes multiple helicity of the magnetic field components, therefore, it is larger than the single helicity estimation given in Ref.[8]. The radial electric field for low density ECH plasmas is positive, and the so-called "electron root" solution is realized. On the other hand, for NBI-heated higher density plasmas, the electric field becomes negative and the "ion root" solution is obtained. From FIGs.2(a)-(c), it is apparent that the experimental electron thermal conductivity near the plasma center is neoclassical for ECH plasmas, while, the transport of NBI plasmas is anomalous in the whole plasma region. As for anomalous empirical transport model combined with neoclassical model, the best fitting s value for low density ECH plasma case (FIG.2(a)) is - 0.4 and the obtained diffusivity is

$$\chi_{emp}(\rho) = 0.57 f_{enh}^{-0.45} P_{MW}^{0.81} B_T^{-0.38} R_m^{-0.89} T_{keV}(\rho)^{-0.55} n_{20}(\rho)^{-0.86}, \qquad (38)$$

and the optimal s value for NBI-heated plasmas (FIG.2(c)) is 0. and the resultant diffusivity is

$$\chi_{emp}(\rho) = 1.47 f_{enh}^{-1} P_{MW}^{0.58} B_T^{-0.84} R_m^{-0.75} n_{20}(\rho)^{-0.69}. \quad (39)$$

As for DWT models , the diffusivity of the collisionless trapped electron mode due to toroidicity (CTEt) is almost same as that due to helicity (CTEh), and the total CTE mode combining the ITG mode roughly agrees with the experimental data. However, in the present CHS parameters CTE modes are stabilized and dissipative (DTE) modes are dominant, since $\nu_{eff t} > \omega_{*e}$. The electrostatic dissipative DWT transport combined with ITG modes does not explain the experimental data, different from ATF results[6].

The electromagnetic mode related with toroidicity (EMt) is close to the experimental transport coefficient for ECH plasmas. These modes for helical ripple (EMh)adopted here is too large and is unrealistic. For NBI-heated plasmas, even the EM mode does not fitted to the experiments near the center.

5. TRANSPORT SIMULATIONS FOR THE LARGE HELICAL DEVICE

5.1 Simulation Model

For the analysis of the LHD transport, a 2.0-dimensional equilibrium-transport code has been developed in which 3D-equilibrium code VMEC [25] and 1D-transport code HTRANS are used. The NBI deposition is calculated by the HFREYA code which is a helical modification of FREYA code[26]) and the slowing-down calculations is done with a Fokker-Planck code FIFPC[27]. The neoclassical transports and anomalous transports as described in Sections 2 and 3 are used. The schematic flow chart of this simulation code is shown in FIG.3.

(1) Equilibrium Analysis

The initial vacuum magnetic surface is calculated by the magnetic tracing code HSD[29] with carefully arranged multi-filament currents. In this paper, the fixed boundary version of VMEC code is used, and the FCT and bootstrap currents are not included. These currents are estimated not enough large to affect the present transport analysis. A full transport simulation which employs the free boundary VMEC code and includes the current equation is under progress. The 3-dimensional magnetic field obtained by the finite beta equilibrium of VMEC is used to evaluate the NBI heat deposition and the multiple-helicity neoclassical coefficients.

(2) Transport Equations

The one-dimensional particle and energy fluid transport equations are of the general form

$$\frac{\partial n_e}{\partial t} = -\frac{1}{V'(\rho)}\frac{\partial}{\partial \rho}[V'(\rho)\Gamma_e] + S_e - \Gamma_{\|e}/L_{\|} \tag{40}$$

$$\frac{\partial}{\partial t}(\frac{3}{2}n_eT_e) = -\frac{1}{V'(\rho)}\frac{\partial}{\partial \rho}[V'(\rho)(Q_e + \frac{5}{2}T_e\Gamma_e)] - \Gamma_e E_r - P_{ei} + P_{He} - P_{rad} - Q_{\|e}/L_{\|} \tag{41}$$

$$\frac{\partial}{\partial t}(\frac{3}{2}n_iT_i) = -\frac{1}{V'(\rho)}\frac{\partial}{\partial \rho}[V'(\rho)(Q_i + \frac{5}{2}T_i\Gamma_i)] + \Gamma_i E_r + P_{ei} + P_{Hi} - P_{cx} - Q_{\|i}/L_{\|} \tag{42}$$

where, S_e denotes the particle source due to the neutral beam fueling and the feedback controlled gas puffing calculated by the Monte-Carlo code AURORA[28]. The variables P_{He} and P_{Hi} are the input heating power to electrons and ions from the neutral beam calculated by Fokker-Planck code[27] and/or the RF heating. P_{ei}, P_{rad} and P_{cx} are the electron-ion power exchange, the radiation power loss, and the charge exchange power loss, respectively. The particle flux Γ and heat flux Q are defined by using diffusion coefficient D and thermal diffusivity χ .

$$\Gamma_e = \Gamma_{ASYe} - (D_{SYMe} + D_{ANe}) <| \nabla\rho |^2> \frac{\partial n_e}{\partial \rho} \tag{43}$$

$$Q_e = Q_{ASYe} - (\chi_{SYMe} + \chi_{ANe})n_e <| \nabla\rho |^2> \frac{\partial T_e}{\partial \rho} \tag{44}$$

$$Q_i = Q_{ASYi} - (\chi_{SYMi} + \chi_{ANi})n_i <| \nabla\rho |^2> \frac{\partial T_i}{\partial \rho} \tag{45}$$

The particle and heat flux to the limiter or divertor is related to the sound velocity C_s multiplied by the coefficients $\alpha(= 0.2 \sim 1.0)$ and $\gamma(=\sim 2.9)$,

$$\Gamma_{\|} = n_e\alpha C_s \tag{46}$$

$$Q_{\|e} = 2\gamma n_eT_e\alpha C_s \tag{47}$$

$$Q_{\|i} = 2n_iT_i\alpha C_s \tag{48}$$

which determine the plasma edge temperature with the assumption of the wall temperature (typically ~10 eV).

5.2 Simulation for LHD Plasmas

The LHD magnetic configuration[3,4] is characterized by the $\ell = 2$ heliotron/torsatron with continuous helical coil system. The major radius is 4m (finally determined to 3.9 m) and the magnetic field strength is 4T. The winding law of the helical coil with the major radius R_c and the minor radius a_c is

$$\theta = \frac{m}{\ell}\phi + \alpha_c \sin(\frac{m}{\ell}\phi)$$

$$\gamma_c = \frac{m a_c}{\ell R_c}$$

where γ_c and α_c are coil pitch parameter and pitch modulation parameter,and θ and ϕ are poloidal and toroidal coordinates, respectively. Three sets of poloidal coils are used to produce various shapings of the plasma cross-section, and three block layers of helical coils are energized to change γ value for the control of the plasma size and the divertor layer. A schematic cross-section of the LHD machine is depicted in FIG.4. Typical simulation results of 20 MW NBI-heated LHD plasmas are shown in FIG.5 for (a)low density and (5)high density discharges. Anomalous particle inward flows are not included in the simulations. Then flat or hollow density profiles are obtained. Such hollow density profiles are seen in many of the existing experiments. For electron thermal transport, the empirical thermal conductivity overweights the neoclassical value; on the other hand, for ion energy transport the neoclassical helical-ripple contribution can not be neglected. Typical predictions from the DWT model with neoclassical transports are presented in Ref. [3]. Because of the flat density profile, the ion temperature gradient (ITG) mode is dominant in the ion transport process of the plasma core, instead of CTE, DTE, CCE and XCE modes.

In order to assess the ripple transport effects, the simulation results without and with ripple transport are compared in FIG.6 (a) and (b). Inclusion of the ripple transport loss leads to the 20 % reduction in the global confinement time. The average temperature is not different, but the central ion temperature is decreased 20 %. The central density is decreased due to the ripple diffusion process. By changing the magnetic configuration from (b) $\alpha_c = 0$ to (c) $\alpha_c = 0.1$, the plasma radius defined by the last closed surface is enlarged from 0.55 cm to 0.60 cm for the case of the inward axis shift of $\Delta_{axis} = -0.1$ m. This moderate positive pitch modulation of the helical coil reduces the central temperature by 20 % because of high ripple ion loss, but leads to a slight increase in the plasma radius and hence, a increase in the global confinement. Moreover, the positive α_c configuration with higher effective helical ripple provides easier access to the hot ion regime with positive

electric field at the low density operation, as shown in FIG.5(a). The higher $nT\tau_E$ value in LHD is achieved by adding positive pitch modulation to get larger plasma volume, instead of negative pitch modulation which is favorable to the neoclassical transport. The final magnetic configuration for LHD was determined by several physics criteria [3] on beta, high-energy particle orbit confinement, divertor configuration, plasma transport, and also on engineering constraints[29].

To reduce the ripple transport and improve the plasma confinement in LHD, the inward-shifting of the plasma column is effective as demonstrated in several recent helical device experiments. In our simulation, the reduction of the ripple loss is included as described in Section 2. The achievable $nT\tau_E$ is plotted as a function of the magnetic axis shift Δ_{axis} for several enhancement factor f_{enh} in FIG.7. The neoclassical loss dominant plasma with $f_{enh} = 10$ is improved obviously (almost twice $nT\tau_E$) by the inward shift. For $f_{enh} = 1$ the fusion product $nT\tau_E$ increases 50 % by the inward axis shift of 0.2 m.

6. SUMMARY

In order to predict LHD (Large Helical Device) plasmas, a new 3-D(dimensional) equilibrium / 1-D transport simulation model for helical confinement systems has been developed. For the transport processes, we have considered the neoclassical transport theory including the effect of radial electric field and multi-helicity magnetic components, and the drift wave turbulence transport for electrostatic and electromagnetic modes, or the anomalous semi-empirical transport. These electron thermal diffusivities are compared with CHS (Compact Helical System) experimental data,

Finally, we have come to the following conclusions:

(1) According to the comparison between the CHS experiment and the present model, the central transport coefficient of the ECH plasma agrees with the neoclassical axi-symmetric value and the transport outside the half radius is anomalous. On the other hand, the transport of NBI-heated plasmas is anomalous in the whole plasma region. It is impossible to explain this anomaly completely by the electrostatic drift wave turbulence models such as dissipative trapped electron modes for CHS flat-density-profile discharges.

(2) In the LHD simulation, it is clarified that the global confinement time is sensitive to the electron anomalous transport. The effect of the neoclassical transport on the global confinement time is around 10 %, however, the central ion temperature can be raised 20 %larger by the reduction of ripple transport. When the anomalous loss can be reduced to the half level of the present scaling, like so-called "H-mode" of the tokamak discharges, the

neoclassical ripple loss through the ion channel becomes important even in the plasma core.

(3) The reduction of anomalous loss is important in LHD and the moderate positive pitch modulation to increase the plasma radius is effective to improve the global confinement rather than the sophisticated neoclassical transport optimization.

(4) The radial inward shift of the plasma column is effective for improving ion confinement and raising the central ion temperature, by reducing this neoclassical asymmetric ion transport loss as well as increasing the plasma radius.

ACKNOWLEDGMENTS

The authors would like to thank Dr. S. P. Hirshman for providing us with the VMEC code, and Dr. C. L. Hedric for the GIOTA code. They also wish to thank Dr. Y. Ogawa for discussing DKES code results, and Drs. H. Yamada, H. Iguchi, K. Ida, and K. Matsuoka for discussing CHS experimental data. They are grateful to Drs. O. Motojima, M. Fujiwara and A. Iiyoshi for continuous encouragements.

References

[1] LYON,A., Fusion Tech. **17**(1990)17.

[2] IIYOSHI,A., FUJIWARA,M., MOTOJIMA,O., OHYABU,N., YAMAZAKI,K., Fusion Tech. **17**(1990)169.

[3] YAMAZAKI,K., OHYABU,N., OKAMOTO,M., AMANO,T., TODOROKI,J., OGAWA,Y., NAKAJIMA,N., et al., in Plasma Physics and Controlled Nuclear Fusion Research 1990 (Proc. 13th Int. Conf. Washington, 1990) IAEA-CN-53/C-4-11.

[4] MOTOJIMA,O., AKAISHI,K., ASAO,M., FUJII,J., et al., in Plasma Physics and Controlled Nuclear Fusion Research 1990 (Proc. 13th Int. Conf. Washington, 1990) IAEA-CN-53/G-1-5.

[5] SUDO,S., TAKEIRI,Y., ZUSHI,H., SANO,F., ITOH,K., KONDO,K., IIYOSHI,A., Nucl. Fusion **30**(1990)11.

[6] MURAKAMI,M., ACETO,S.C., ANABITARTE,E., ANDERSON,D.T., et al., in Plasma Physics and Controlled Nuclear Fusion Research 1990 (Proc. 13th Int. Conf. Washington, 1990) IAEA-CN-53/C-1-3 .

[7] ZUSHI,H., et al., Nucl. Fusion **24**(1984)305.

[8] IGUCHI,H., HOSOKAWA,M., HOWE,H.C., IDA,K., IDEI,H., KANEKO,O., et al., in Controlled Fusion and Plasma Heating (Proc. 16th Europ. Conf. Amsterdam, 1990), Vol.2, European Physical Society (1990) 451.

[9] SANO,F., TAKEIRI,Y., HANATANI,K., ZUSHI,H., SATO,M., SUDO,S., et al., Nucl. Fusion **30** (1990)81.

[10] RINGLER,H., GASPARINO,U., KUHER,G., MAASSBERG,H., RENNER,H., et al., Plasma Phys. Controlled Fusion **32**(1990)933.

[11] HINTON,F.L., HAZELTINE,R.D., Rev. Mod. Phys. **48**(1976)239.

[12] CHANG,C.S., HINTON,F.L., Phys. Fluids **25**(1982)1493.

[13] SHAING, K.C., CALLEN, J.D., Phys. Fluids **26**(1983)3315.

[14] CRUME,E.C., SHAIN,K.C., HIRSHMAN,S.P.,van RIJ,W.I., Phys.Fluids **31**(1988)11.

[15] HASTING,D.E., HOULBERG,W.A., SHAING,K.C., Nucl. Fusion **25**(1985)445.

[16] SHAING,K.C., HORKIN,S.A., Phys. Fluids **26**(1983)2136.

[17] HEDRIC,C.L., private communication on the GIOTA code.

[18] HIRSHMAN,S.P., et al., Phys. Fluids, **29**(1986)2951.

[19] PERKINS,F.W, in Heating in Toroidal Plasmas (Proc. 4th Int. Symp. Rome, 1984), Vol.1, Int. School of Plasma Physics, Varena(1984)97.

[20] DOMINGUEZ,R.R., WALTZ,R.E., Nucl. Fusion **27**(1984)65.

[21] GOLDSTON,R., Bull. Am. Phys. Soc.34(1989)1964.

[22] HORTON,W., BEKKI,N., BERK,L.H. et al., in Plasma Physics and Controlled Nuclear Fusion Research 1990 (Proc. 12th Int. Conf. Nice, 1988) Vol.2, p.211 (1989) IAEA-CN-53/C-4-11.

[23] OHKAWA,T., Phys. Lett. 67A(1978)35.

[24] IDA,K., YAMADA,H., IGUCHI,H., HIDEKUMA,S., SANUKI, H., YAMAZAKI,K., the CHS Group, Phys. Fluids B**3**(1991)515.

[25] HIRSHMAN,S.P., van RIJ, W.I., MERKEL, P., Comput. Phys. Commun. **43**(1986)143.

[26] LISTER,G.G., POST,D.E., GOLDSTON,R. in Third Sympo. Plasma Heating in Toroidal Devices, p.303, ed by E.Sindoni (1976)

[27] FOWLER,R.H., SMITH,J., ROME,J.A., Comput. Phys. Commun. **13**(1978)323.

[28] HUGES,M.H., POST,D.E., J. Comput. Phys. **28**(1978)43.

[29] YAMAZAKI,K., MOTOJIMA,O., ASAO,M., FUJIWARA,M., IIYOSHI,A., National Institute for Fusion Science Research Report NIFS-30(1990).

FIGURE CAPTIONS

FIG.1 Schematic drawing of transport coefficients for drift wave turbulence model. The collisionless or collisional circulating electron mode (CCE or XCE), the collisionless or dissipative trapped electron mode due to toroidicity (CTEt or DTEt), the collisionless or dissipative trapped electron mode due to helicity (CTEh or DTEh), the ion temperature mode (ITG) and the electromagnetic mode (EM) are shown as a function of the collision frequency ν_{ei}.

FIG.2 Comparisons of modeled thermal conductivities with CHS experimental data[8].

Top figures of density profile n_e and temperature profiles T_e, T_i are obtained from experimental data, and the radial electric field profiles E_ρ in the second figure are calculated using the ripple transport model. The experimental diffusivity (CHS Exp.) is compared with semi-empirical model combined with neoclassical transport(emp+NC) with several s value in the lower figure. The drift wave models are also compared in the lowest figures.

(a) low density ECH case

(b) medium density ECH case

(c) NBI-heated case

FIG.3 Flow chart of equilibrium-transport simulation analysis.

The 3-D equilibrium VMEC code is coupled in the FCT manner to the 1-D transport code HTRANS including neoclassical ripple transport GIOTA and various NBI heating codes.

FIG.4 LHD machine configuration and plasma equilibrium.

Helical pitch M= 10,

Major raidus R= 4.0 m,

Toroidal field B= 4.0 T.

FIG.5 Transport simulations of LHD plasmas in 20 MW NBI heating case.

(a) Low density case with positive electric field (Electron Root),

(average electron density: $3.0 \times 10^{19}\mathrm{m}^{-3}$)

(b) High density case with negative electric field (Ion Root).

(average electron density: $1.0 \times 10^{20}\mathrm{m}^{-3}$)

FIG.6 Effects of the helical ripple transport and the magnetic configuration.

(a) Without helical ripple diffusion

Empirical anomalous model with symmetric neoclassical transport is taken into account.

(b) Standard configuration case ($\alpha_c = 0.0$) with empirical anomalous loss and neoclassical total loss

(c) Positive helical pitch modulation ($\alpha_c = 0.1$) with empirical anomalous loss and neoclassical total loss

FIG.7 Effects of the radial inward shift Δ_{axis} and the confinement enhancement factor f_{enh} on the central value of the fusion product $n(0)T(0)\tau_E$.

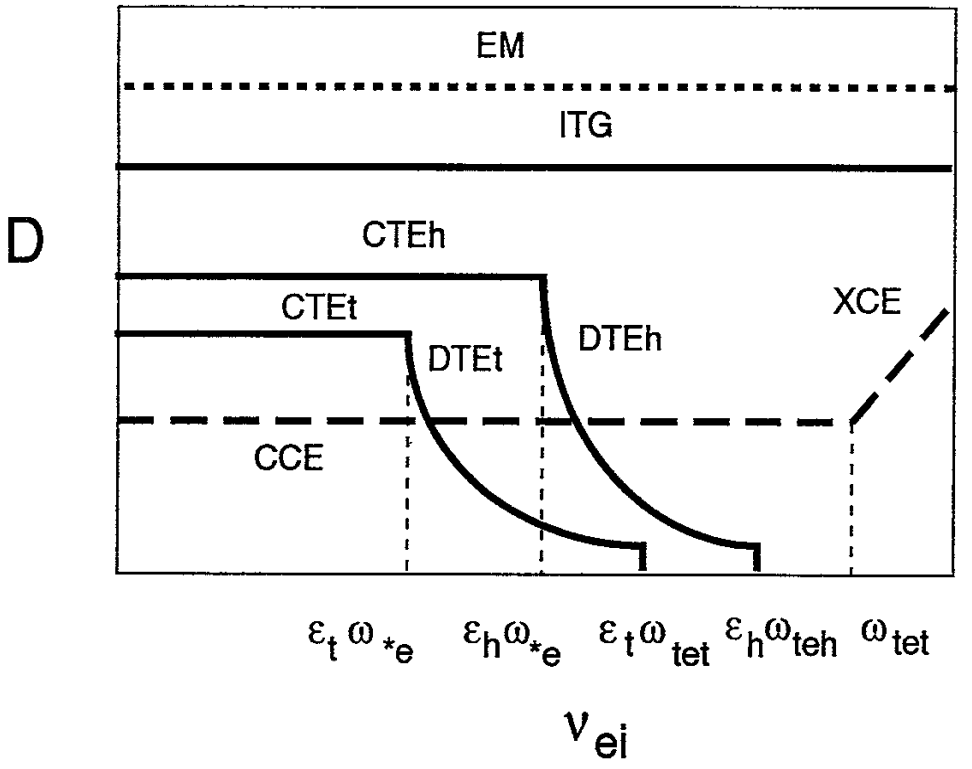
D
EM
ITG
CTEh
CTEt
DTEt
DTEh
XCE
CCE
$\varepsilon_t \omega_{*e}$
$\varepsilon_h \omega_{*e}$
$\varepsilon_t \omega_{tet}$
$\varepsilon_h \omega_{teh}$
ω_{tet}
ν_{ei}

FIG. 1

(a)

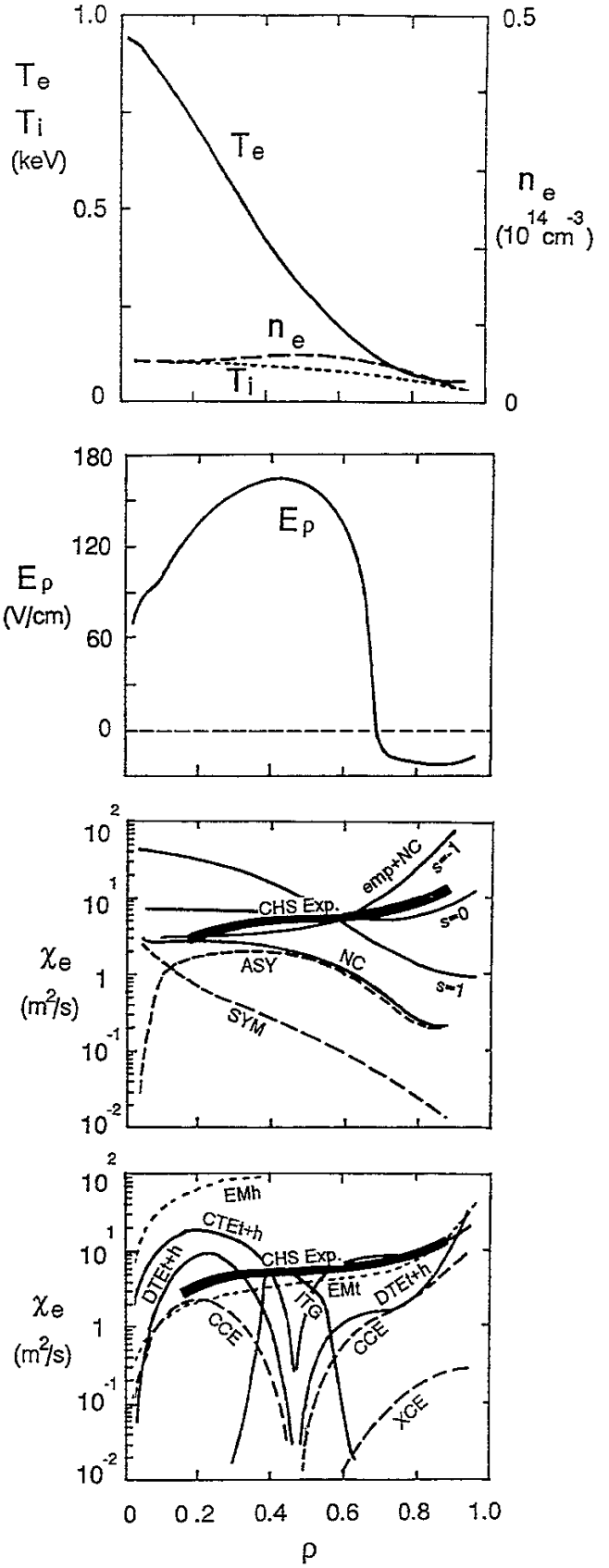
1.0
0.5
0
Te
Ti
(keV)
Te
ne
Ti
0.5
ne
(10^14 cm^-3)
0
180
120
60
0
Ep
(V/cm)
Ep
10^2
10^1
1
10^-1
10^-2
χe
(m^2/s)
emp+NC
s=-1
CHS Exp.
s=0
ASY
NC
s=1
SYM
EMh
CTEt+h
DTEt+h
CHS Exp.
EMt
ITG
DTEt+h
CCE
CCE
XCE
0
0.2
0.4
0.6
0.8
1.0
ρ

FIG. 2 (a)

(b)

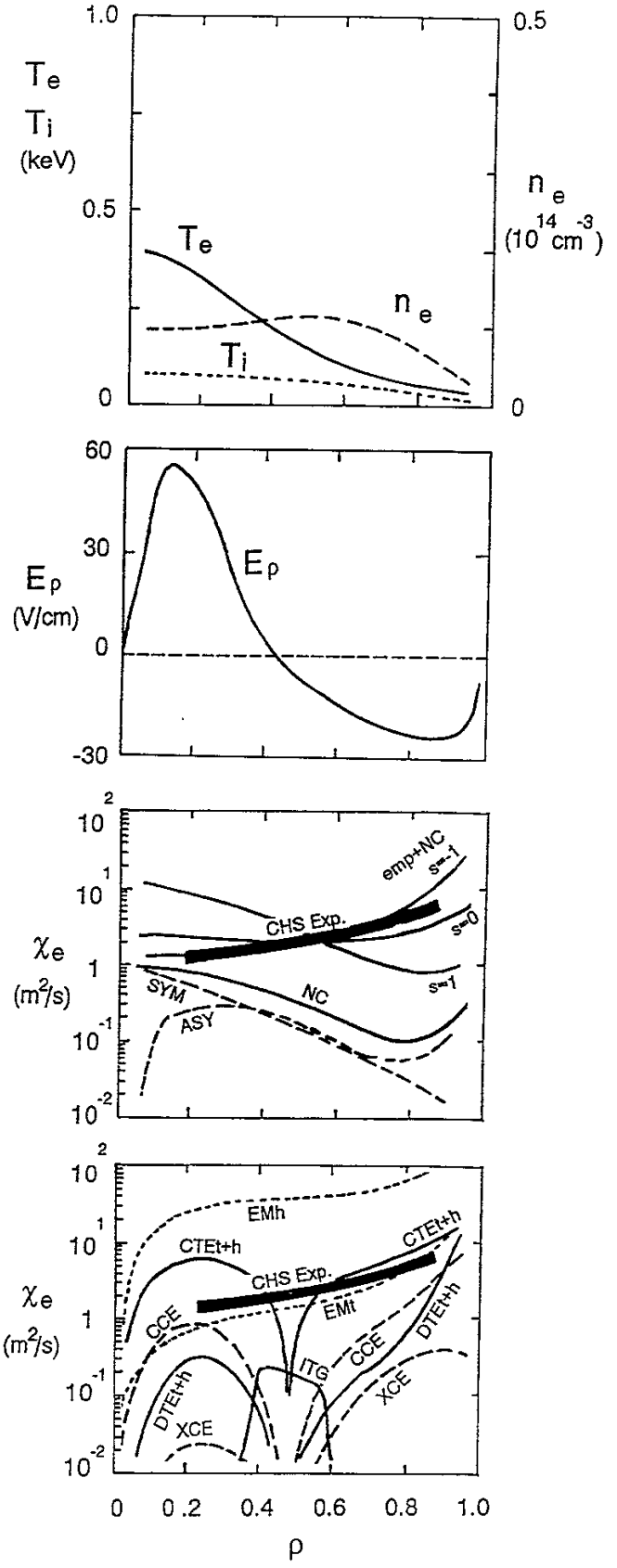
1.0
0.5
Te
Ti
(keV)
0.5
Te
ne
Ti
0
0.5
ne
(10^14 cm^-3)
0
60
30
Eρ
(V/cm)
0
-30
Eρ
10^2
10^1
1
10^-1
10^-2
χe
(m^2/s)
emp+NC
s=-1
CHS Exp.
s=0
s=1
SYM
NC
ASY
10^2
10^1
1
10^-1
10^-2
χe
(m^2/s)
EMh
CTEt+h
CTEt+h
CHS Exp.
EMt
CCE
ITG
CCE
DTEt+h
DTEt+h
XCE
XCE
0
0.2
0.4
0.6
0.8
1.0
ρ

FIG. 2 (b)

(c)

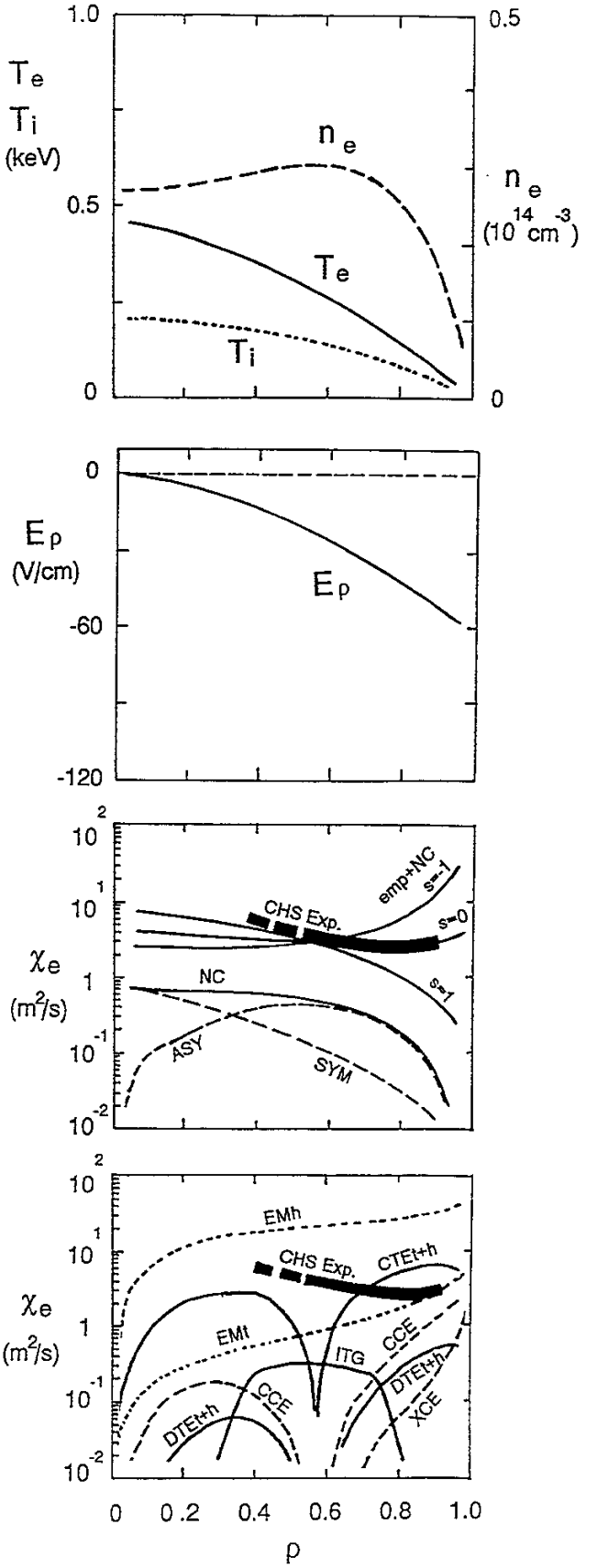
1.0
0.5
0
Te
Ti
(keV)
ne
Te
Ti
ne
(10^14 cm^-3)
0.5
0
0
-60
-120
Ep
(V/cm)
Ep
10^2
10^1
1
10^-1
10^-2
χe
(m^2/s)
emp+NC
s=-1
CHS Exp.
s=0
s=1
NC
ASY
SYM
EMh
CHS Exp.
CTEt+h
EMi
ITG
CCE
DTEt+h
CCE
DTEt+h
XCE
0
0.2
0.4
0.6
0.8
1.0
ρ

FIG. 2 (c)

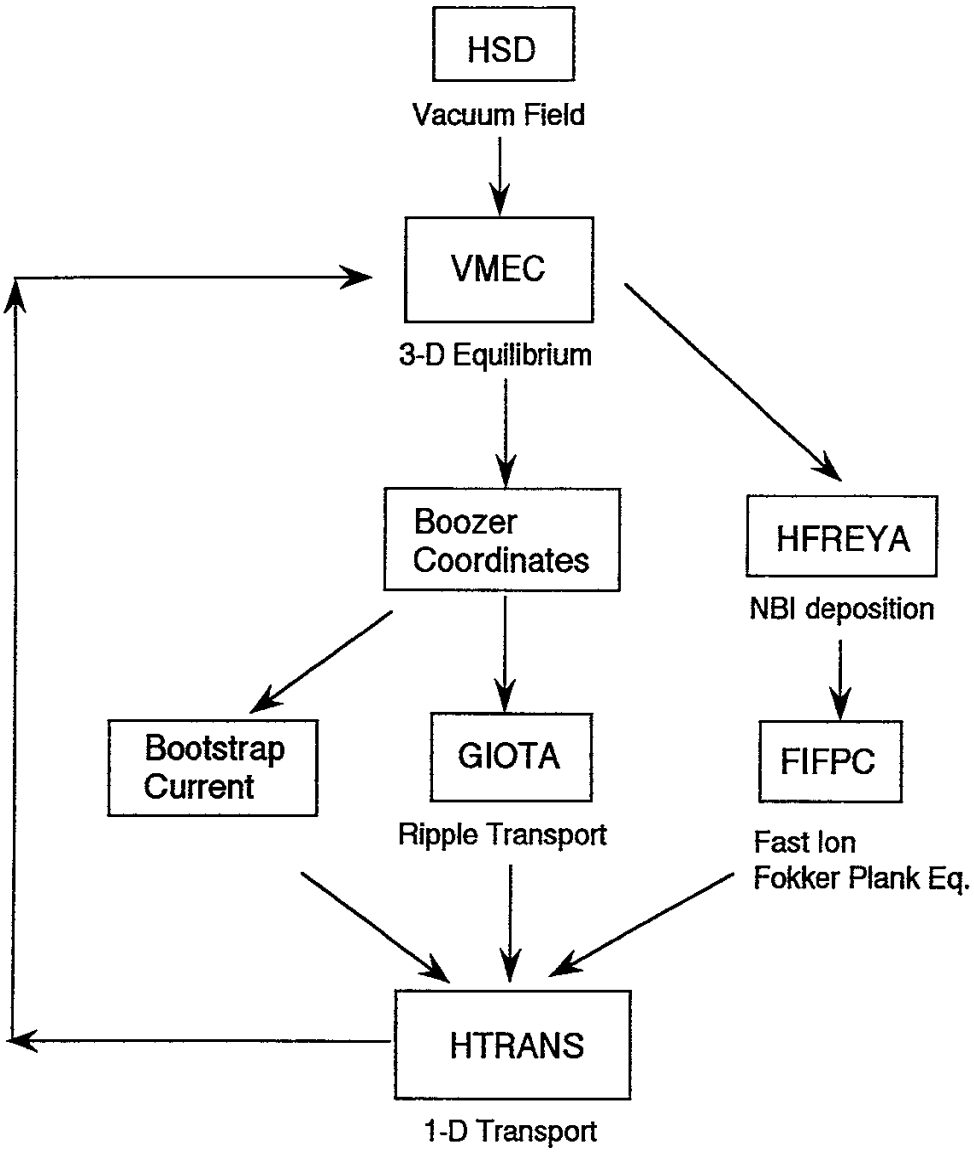
HSD
Vacuum Field
VMEC
3-D Equilibrium
Boozer Coordinates
HFREYA
NBI deposition
Bootstrap Current
GIOTA
Ripple Transport
FIFPC
Fast Ion Fokker Plank Eq.
HTRANS
1-D Transport

FIG. 3

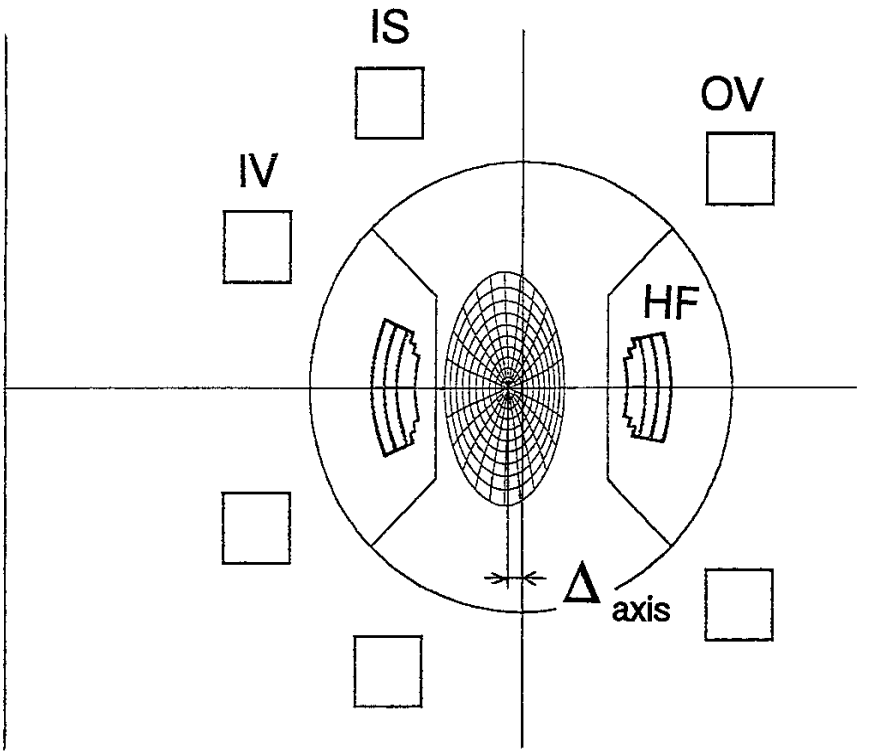

FIG. 4

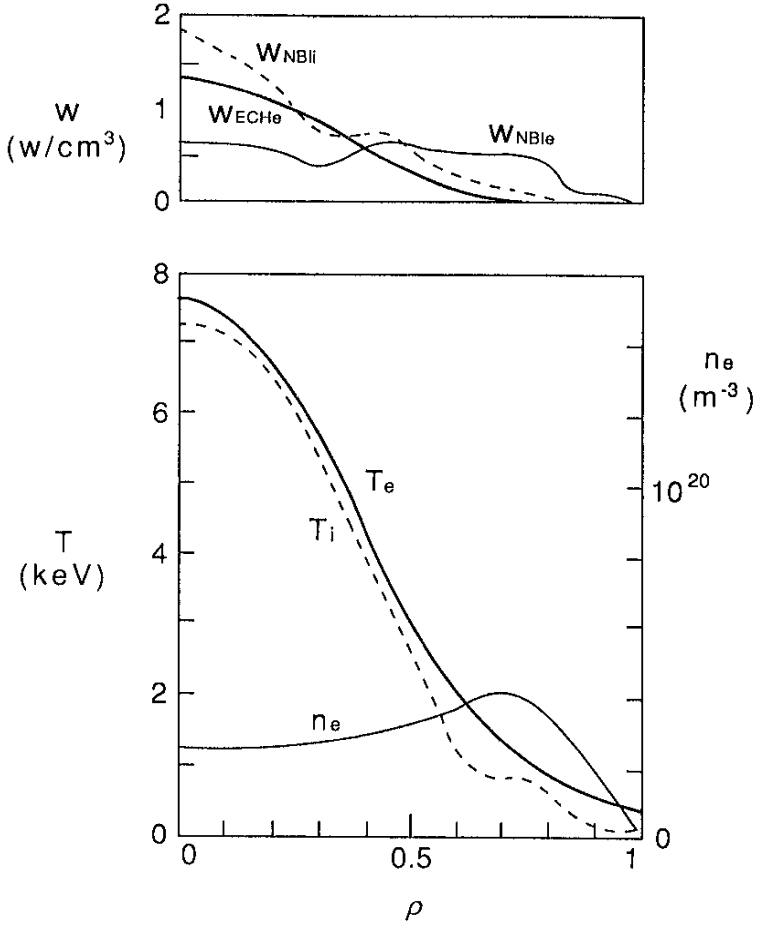
W
(w/cm³)
W_NBIi
W_ECHe
W_NBIe
T
(keV)
T_e
T_i
n_e
n_e
(m⁻³)
10²⁰
ρ

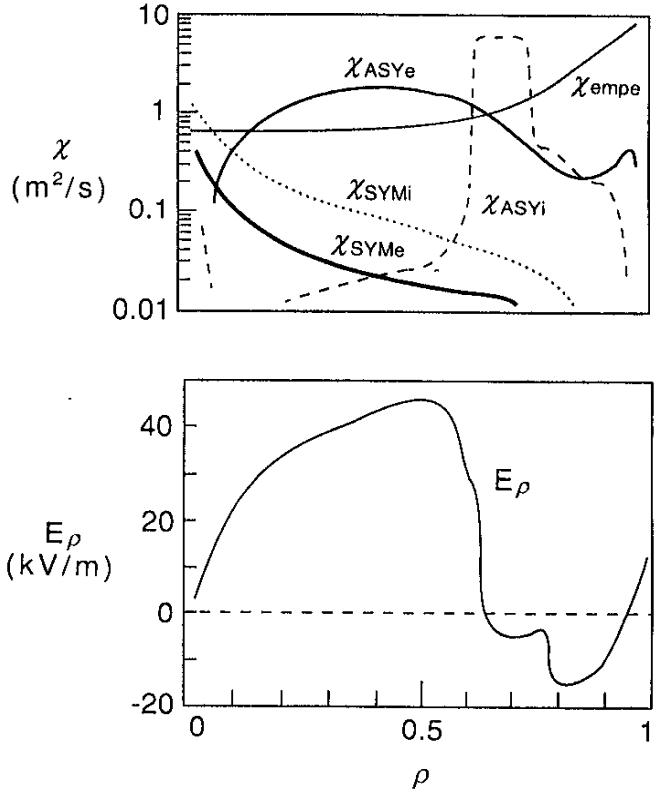
χ
(m²/s)
χ_ASYe
χ_empe
χ_SYMi
χ_ASYi
χ_SYMe
E_ρ
(kV/m)
E_ρ
ρ

FIG. 5 (a)

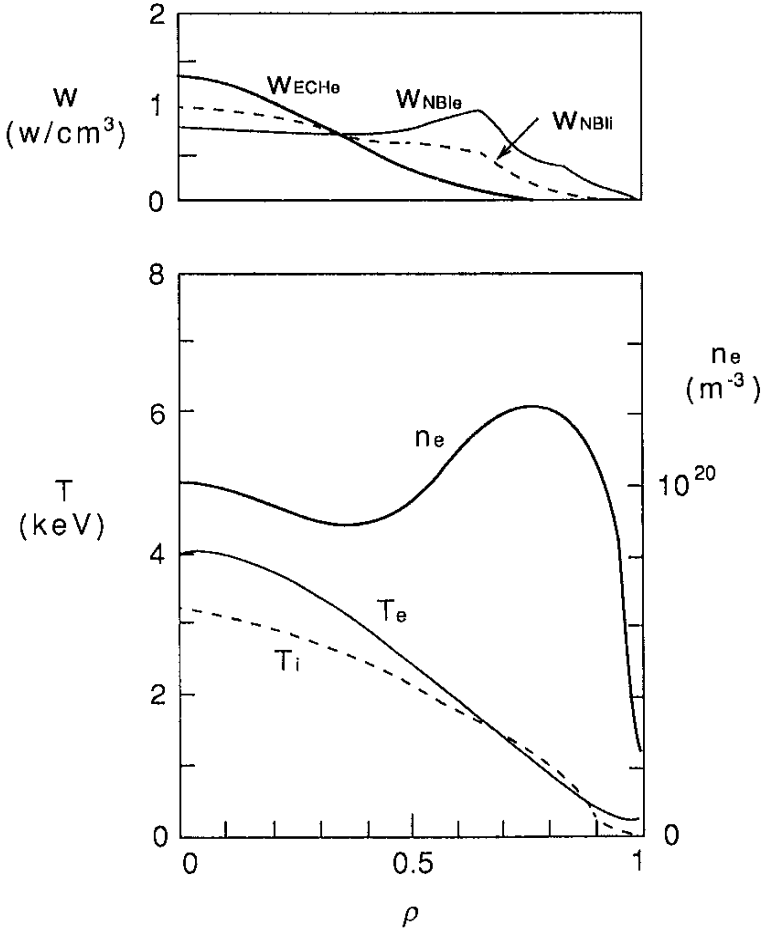
W
(w/cm³)
2
1
0
WECHe
WNBIe
WNBIi
T
(keV)
8
6
4
2
0
ne
(m⁻³)
10²⁰
0
ne
Te
Ti
0
0.5
1
ρ

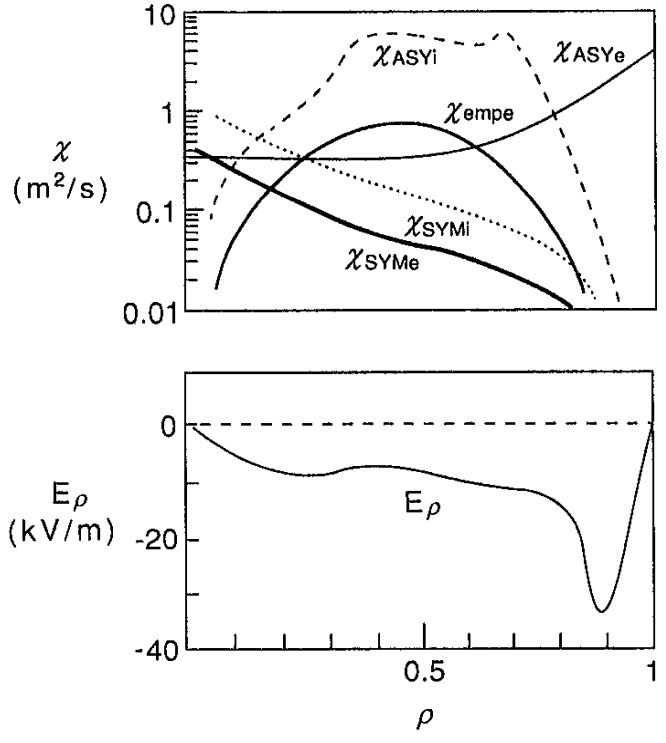
χ
(m²/s)
10
1
0.1
0.01
χASYi
χASYe
χempe
χSYMi
χSYMe
Eρ
(kV/m)
0
-20
-40
Eρ
0.5
1
ρ

FIG. 5 (b)

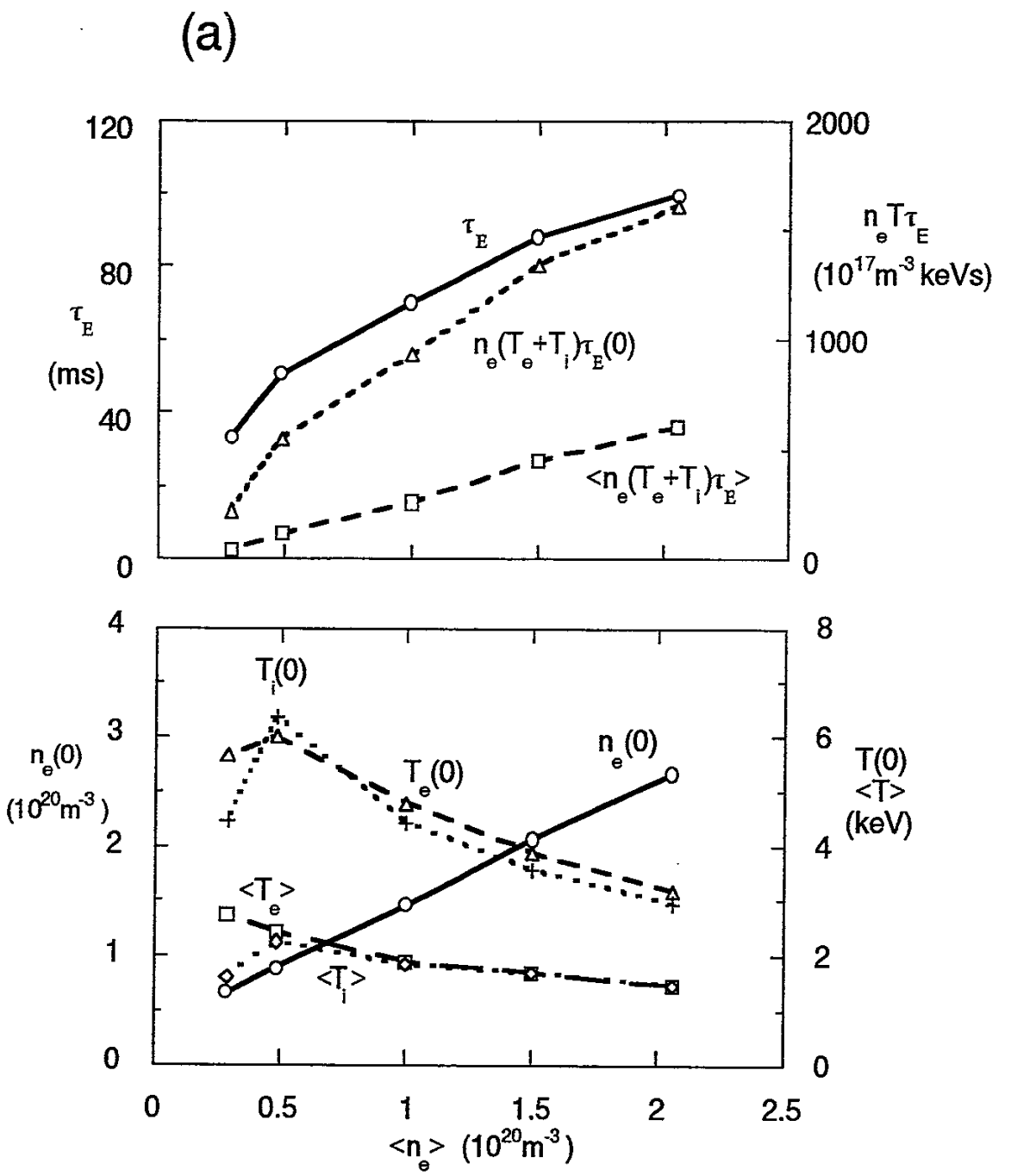
(a)
120
80
40
0
τ_E
(ms)
2000
1000
0
$n_e T \tau_E$
($10^{17} m^{-3}$ keVs)
τ_E
$n_e(T_e+T_i)\tau_E(0)$
$<n_e(T_e+T_i)\tau_E>$
4
3
2
1
0
$n_e(0)$
($10^{20} m^{-3}$)
8
6
4
2
0
T(0)
<T>
(keV)
$T_i(0)$
$T_e(0)$
$n_e(0)$
$<T_e>$
$<T_i>$
0
0.5
1
1.5
2
2.5
$<n_e>$ ($10^{20} m^{-3}$)

FIG. 6 (a)

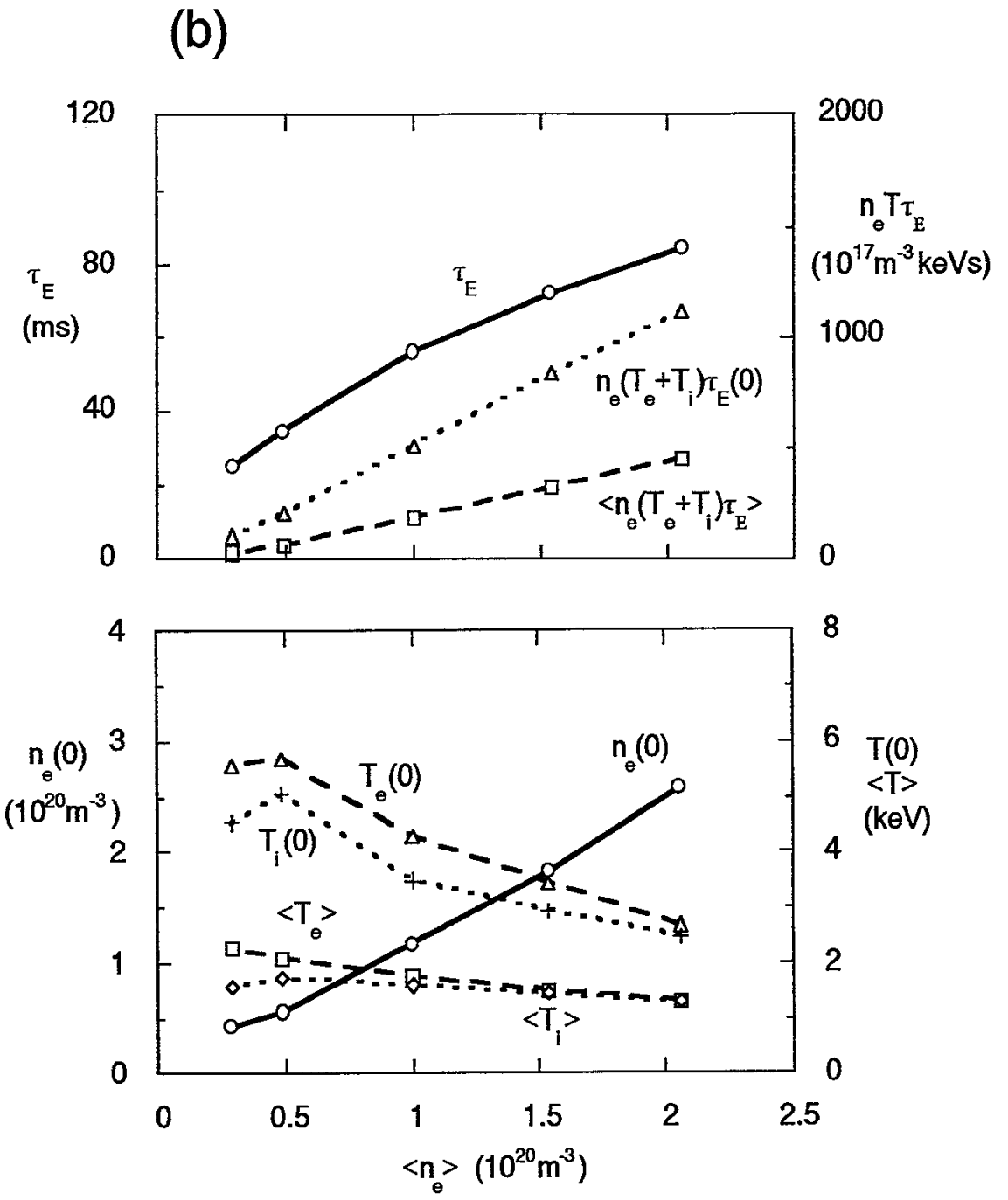
(b)
120
80
40
0
2000
1000
0
τ_E (ms)
$n_e T \tau_E$ ($10^{17} m^{-3} keVs$)
τ_E
$n_e(T_e+T_i)\tau_E(0)$
$<n_e(T_e+T_i)\tau_E>$
4
3
2
1
0
8
6
4
2
0
$n_e(0)$ ($10^{20} m^{-3}$)
T(0) <T> (keV)
$T_e(0)$
$T_i(0)$
$n_e(0)$
$<T_e>$
$<T_i>$
0
0.5
1
1.5
2
2.5
$<n_e>$ ($10^{20} m^{-3}$)

FIG. 6 (b)

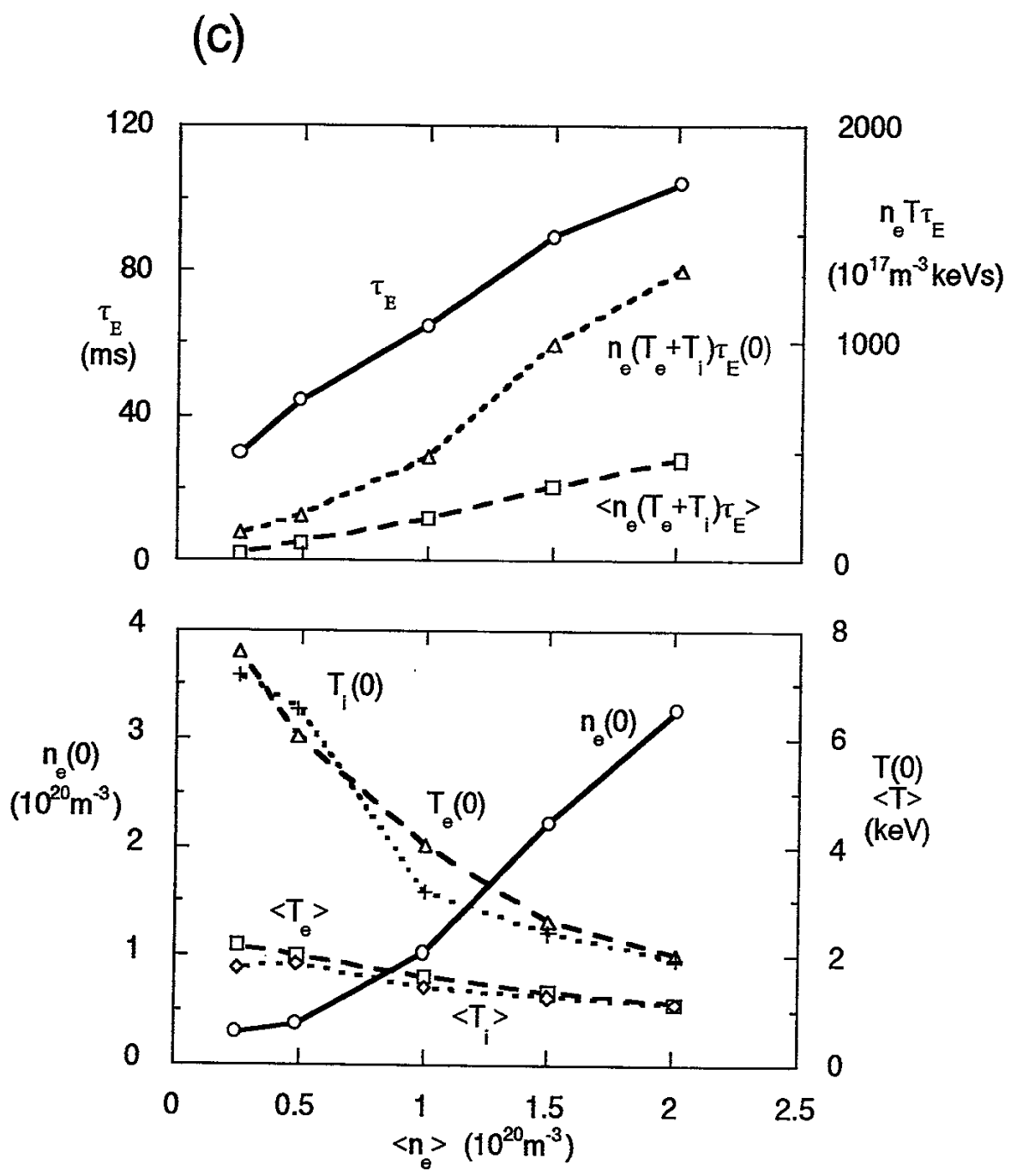
(c)
120
80
40
0
τ_E (ms)
τ_E
$n_e(T_e+T_i)\tau_E(0)$
$<n_e(T_e+T_i)\tau_E>$
2000
1000
0
$n_e T\tau_E$ ($10^{17}m^{-3}keVs$)
4
3
2
1
0
$n_e(0)$ ($10^{20}m^{-3}$)
$T_i(0)$
$n_e(0)$
$T_e(0)$
$<T_e>$
$<T_i>$
8
6
4
2
0
T(0) <T> (keV)
0
0.5
1
1.5
2
2.5
$<n_e>$ ($10^{20}m^{-3}$)

FIG. 6 (c)

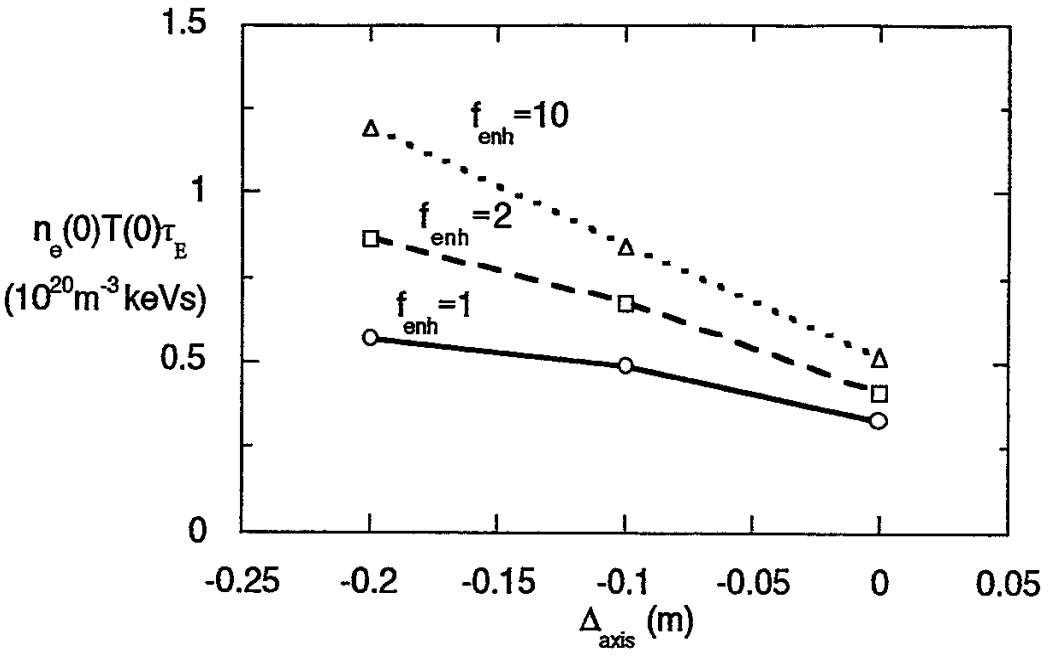
1.5
1
0.5
0
$n_e(0)T(0)\tau_E$
$(10^{20}m^{-3}keVs)$
$f_{enh}=10$
$f_{enh}=2$
$f_{enh}=1$
-0.25
-0.2
-0.15
-0.1
-0.05
0
0.05
Δ_{axis} (m)

FIG. 7

Recent Issues of NIFS Series

NIFS-47 Yoshi H.Ichikawa, *Solitons and Chaos in Plasma*; Sep. 1990

NIFS-48 T.Seki, R.Kumazawa, Y.Takase, A.Fukuyama, T.Watari, A.Ando, Y.Oka, O.Kaneko, K.Adati, R.Akiyama, R.Ando, T.Aoki, Y.Hamada, S.Hidekuma, S.Hirokura, K.Ida, K.Itoh, S.-I.Itoh, E.Kako, A. Karita, K.Kawahata, T.Kawamoto, Y.Kawasumi, S.Kitagawa, Y.Kitoh, M.Kojima, T.Kuroda, K.Masai, S.Morita, K.Narihara, Y.Ogawa, K.Ohkubo, S.Okajima, T.Ozaki, M.Sakamoto, M.Sasao, K.Sato, K.N.Sato, F.Shinbo, H.Takahashi, S.Tanahashi, Y.Taniguchi, K.Toi and T.Tsuzuki, *Application of Intermediate Frequency Range Fast Wave to JIPP T-IIU Plasma*; Sep.1990

NIFS-49 A.Kageyama, K.Watanabe and T.Sato, *Global Simulation of the Magnetosphere with a Long Tail: The Formation and Ejection of Plasmoids*; Sep.1990

NIFS-50 S.Koide, *3-Dimensional Simulation of Dynamo Effect of Reversed Field Pinch*; Sep. 1990

NIFS-51 O.Motojima, K. Akaishi, M.Asao, K.Fujii, J.Fujita, T.Hino, Y.Hamada, H.Kaneko, S.Kitagawa, Y.Kubota, T.Kuroda, T.Mito, S.Morimoto, N.Noda, Y.Ogawa, I.Ohtake, N.Ohyabu, A.Sagara, T. Satow, K.Takahata, M.Takeo, S.Tanahashi, T.Tsuzuki, S.Yamada, J.Yamamoto, K.Yamazaki, N.Yanagi, H.Yonezu, M.Fujiwara, A.Iiyoshi and LHD Design Group, *Engineering Design Study of Superconducting Large Helical Device*; Sep. 1990

NIFS-52 T.Sato, R.Horiuchi, K. Watanabe, T. Hayashi and K.Kusano, *Self-Organizing Magnetohydrodynamic Plasma*; Sep. 1990

NIFS-53 M.Okamoto and N.Nakajima, *Bootstrap Currents in Stellarators and Tokamaks*; Sep. 1990

NIFS-54 K.Itoh and S.-I.Itoh, *Peaked-Density Profile Mode and Improved Confinement in Helical Systems*; Oct. 1990

NIFS-55 Y.Ueda, T.Enomoto and H.B.Stewart, *Chaotic Transients and Fractal Structures Governing Coupled Swing Dynamics*; Oct. 1990

NIFS-56 H.B.Stewart and Y.Ueda, *Catastrophes with Indeterminate Outcome*; Oct. 1990

NIFS-57 S.-I.Itoh, H.Maeda and Y.Miura, *Improved Modes and the Evaluation of Confinement Improvement*; Oct. 1990

NIFS-58 H.Maeda and S.-I.Itoh, *The Significance of Medium- or Small-size Devices in Fusion Research*; Oct. 1990

NIFS-59 A.Fukuyama, S.-I.Itoh, K.Itoh, K.Hamamatsu, V.S.Chan, S.C.Chiu, R.L.Miller and T.Ohkawa, *Nonresonant Current Drive by RF Helicity Injection*; Oct. 1990

NIFS-60 K.Ida, H.Yamada, H.Iguchi, S.Hidekuma, H.Sanuki, K.Yamazaki and CHS Group, *Electric Field Profile of CHS Heliotron/Torsatron Plasma with Tangential Neutral Beam Injection*; Oct. 1990

NIFS-61 T.Yabe and H.Hoshino, *Two- and Three-Dimensional Behavior of Rayleigh-Taylor and Kelvin-Helmholz Instabilities*; Oct. 1990

NIFS-62 H.B. Stewart, *Application of Fixed Point Theory to Chaotic Attractors of Forced Oscillators;* Nov. 1990

NIFS-63 K.Konn., M.Mituhashi, Yoshi H.Ichikawa,*Soliton on Thin Vortex Filament;* Dec. 1990

NIFS-64 K.Itoh, S.-I.Itoh and A.Fukuyama,*Impact of Improved Confinement on Fusion Research;* Dec. 1990

NIFS -65 A.Fukuyama, S.-I.Itoh and K. Itoh,*A Consistency Analysis on the Tokamak Reactor Plasmas;* Dec. 1990

NIFS-66 K.Itoh, H. Sanuki, S.-I. Itoh and K. Tani,*Effect of Radial Electric Field on α-Particle Loss in Tokamaks;* Dec. 1990

NIFS-67 K.Sato,and F.Miyawaki,*Effects of a Nonuniform Open Magnetic Field on the Plasma Presheath*; Jan.1991

NIFS-68 K.Itoh and S.-I.Itoh,*On Relation between Local Transport Coefficient and Global Confinement Scaling Law;* Jan. 1991

NIFS-69 T.Kato, K.Masai, T.Fujimoto,F.Koike, E.Källne, E.S.Marmar and J.E.Rice,*He-like Spectra Through Charge Exchange Processes in Tokamak Plasmas;* Jan.1991

NIFS-70 K. Ida, H. Yamada, H. Iguchi, K. Itoh and CHS Group, *Observation of Parallel Viscosity in the CHS Heliotron/Torsatron* ; Jan.1991

NIFS-71 H. Kaneko, *Spectral Analysis of the Heliotron Field with the Toroidal Harmonic Function in a Study of the Structure of Built-in Divertor* ; Jan. 1991

NIFS-72 S. -I. Itoh, H. Sanuki and K. Itoh, *Effect of Electric Field Inhomogeneities on Drift Wave Instabilities and Anomalous Transport* ; Jan. 1991

NIFS-73 Y.Nomura, Yoshi.H.Ichikawa and W.Horton, *Stabilities of Regular Motion in the Relativistic Standard Map*; Feb. 1991

NIFS-74 T.Yamagishi, *Electrostatic Drift Mode in Toroidal Plasma with Minority Energetic Particles*, Feb. 1991

NIFS-75 T.Yamagishi, *Effect of Energetic Particle Distribution on Bounce Resonance Excitation of the Ideal Ballooning Mode*, Feb. 1991

NIFS-76 T.Hayashi, A.Tadei, N.Ohyabu and T.Sato, *Suppression of Magnetic Surface Breading by Simple Extra Coils in Finite Beta Equilibrium of Helical System;* Feb. 1991

NIFS-77 N. Ohyabu, *High Temperature Divertor Plasma Operation*; Feb. 1991

NIFS-78 K.Kusano, T. Tamano and T. Sato, *Simulation Study of Toroidal Phase-Locking Mechanism in Reversed-Field Pinch Plasma*; Feb. 1991

NIFS-79 K. Nagasaki, K. Itoh and S. -I. Itoh, *Model of Divertor Biasing and Control of Scrape-off Layer and Divertor Plasmas*; Feb. 1991

NIFS-80 K. Nagasaki and K. Itoh, *Decay Process of a Magnetic Island by Forced Reconnection*; Mar. 1991

NIFS-81 K. Takahata, N. Yanagi, T. Mito, J. Yamamoto, O.Motojima and LHDDesign Group, K. Nakamoto, S. Mizukami, K. Kitamura, Y. Wachi, H. Shinohara, K. Yamamoto, M. Shibui, T. Uchida and K. Nakayama, *Design and Fabrication of Forced-Flow Coils as R&D Program for Large Helical Device*; Mar. 1991

NIFS-82 T. Aoki and T. Yabe, *Multi-dimensional Cubic Interpolation for ICF Hydrodynamics Simulation*; Apr. 1991

NIFS-83 K. Ida, S.-I. Itoh, K. Itoh, S. Hidekuma, Y. Miura, H. Kawashima, M. Mori, T. Matsuda, N. Suzuki, H. Tamai, T.Yamauchi and JFT-2M Group, *Density Peaking in the JFT-2M Tokamak Plasma with Counter Neutral Beam Injection* ; May 1991

NIFS-84 A. Iiyoshi, *Development of the Stellarator/Heliotron Research*; May 1991

NIFS-85 Y. Okabe, M. Sasao, H. Yamaoka, M. Wada and J. Fujita, *Dependence of Au^- Production upon the Target Work Function in a Plasma-Sputter-Type Negative Ion Source;* May 1991

NIFS-86 N. Nakajima and M. Okamoto, *Geometrical Effects of the Magnetic Field on the Neoclassical Flow, Current and Rotation in General Toroidal Systems*; May 1991

NIFS-87 S. -I. Itoh, K. Itoh, A. Fukuyama, Y. Miura and JFT-2M Group, *ELMy-H mode as Limit Cycle and Chaotic Oscillations in Tokamak Plasmas;* May 1991

NIFS-88 N.Matsunami and K.Kitoh, *High Resolution Spectroscopy of H^+ Energy Loss in Thin Carbon Film;* May 1991

NIFS-89 H. Sugama, N. Nakajima and M.Wakatani, *Nonlinear Behavior of Multiple-Helicity Resistive Interchange Modes near Marginally Stable States;* May 1991

NIFS-90 H. Hojo and T.Hatori, *Radial Transport Induced by Rotating RF Fields and Breakdown of Intrinsic Ambipolarity in a Magnetic Mirror*; Jun. 1991

NIFS-91 M. Tanaka, S. Murakami, H. Takamaru and T.Sato, *Macroscale Implicit, Electromagnetic Particle Simulation of Inhomogeneous and Magnetized Plasmas in Multi-Dimensions;* Jun. 1991

NIFS-92 S. - I. Itoh, *H-mode Physics, -Experimental Observations and Model Theories-, Lecture Notes, Spring College on Plasma Physics, May 27 - June 21 1991 at International Centre for Theoretical Physics (IAEA UNESCO) Trieste, Italy ;* Jun. 1991

NIFS-93 Y. Miura, K. Itoh, S. - I. Itoh, T. Takizuka, H. Tamai, T. Matsuda, N. Suzuki, M. Mori, H. Maeda and O. Kardaun, *Geometric Dependence of the Scaling Law on the Energy Confinement Time in H-mode Discharges;* Jun. 1991

NIFS-94 H. Sanuki, K. Itoh, K. Ida and S. - I. Itoh, *On Radial Electric Field Structure in CHS Torsatron / Heliotron;* Jun. 1991

NIFS-95 K. Itoh, H. Sanuki and S. - I. Itoh, *Influence of Fast Ion Loss on Radial Electric Field in Wendelstein VII-A Stellarator;* Jun. 1991

NIFS-96 S. - I. Itoh, K. Itoh, A. Fukuyama, *ELMy-H mode as Limit Cycle and Chaotic Oscillations in Tokamak Plasmas;* Jun. 1991

NIFS-97 K. Itoh, S. - I. Itoh, H. Sanuki, A. Fukuyama, *An H-mode-Like Bifurcation in Core Plasma of Stellarators;* Jun. 1991

NIFS-98 H. Hojo, T. Watanabe, M. Inutake, M. Ichimura and S. Miyoshi, *Axial Pressure Profile Effects on Flute Interchange Stability in the Tandem Mirror GAMMA 10;* Jun. 1991

NIFS-99 A. Usadi, A. Kageyama, K. Watanabe and T. Sato, *A Global Simulation of the Magnetosphere with a Long Tail : Southward and Northward IMF;* Jun. 1991

NIFS-100 H. Hojo, T. Ogawa and M. Kono, *Fluid Description of Ponderomotive Force Compatible with the Kinetic One in a Warm Plasma* ; July 1991

NIFS-101 H. Momota, A. Ishida, Y. Kohzaki, G. H. Miley, S. Ohi, M. Ohnishi K. Yoshikawa, K. Sato, L. C. Steinhauer, Y. Tomita and M. Tuszewski *Conceptual Design of D-^{3}He FRC Reactor "ARTEMIS"* ; July 1991

NIFS-102 N. Nakajima and M. Okamoto, *Rotations of Bulk Ions and Impurities in Non-Axisymmetric Toroidal Systems* ; July 1991

NIFS-103 A. J. Lichtenberg, K. Itoh, S. - I. Itoh and A. Fukuyama, *The Role of Stochasticity in Sawtooth Oscillation* ; Aug. 1991